Pergamon

Int. J. Heat Mass Transfer. Vol. 37, No. 12, pp. 1773–1781, 1994

0017-9310/94 $7.00 + 0.00

0017-9310(93)E0106-Q

A numerical study of the effect of Coriolis force on the fluid flow and heat transfer due to wire heating on centrifuge

KYUNG-WOO YI,† SHIN NAKAMURA,‡ TAKETOSHI HIBIYA‡ and KOICHI KAKIMOTO†

†Fundamental Research Laboratories, NEC Corporation, 34 Miyukigaoka, Tsukuba 305, Japan
‡Space Technology Corporation, 34 Miyukigaoka, Tsukuba 305, Japan

(*Received* 19 *July* 1993 *and in final form* 19 *November* 1993)

Abstract—The effects of the Coriolis force on a flow field, and on temperature increase during transient hot-wire heating, were studied by three-dimensional and time-dependent calculation as compared to the experimental result. We have found that the Coriolis force drastically changes the flow field as well as the heat transfer tendencies of mercury on a centrifuge. The origin of these changes is that the Coriolis force reduces the component of velocity parallel to the effective gravity, and increases the radial and azimuthal components normal to the direction of the effective gravity on the centrifuge. The order of the effect of the Coriolis force depends on the configuration and the characteristic length of the specimen.

1. INTRODUCTION

THE UTILIZATION of a centrifuge is the only way to achieve high gravity conditions on earth. Two forces, Coriolis and centrifugal forces, play dominant roles when fluid is rotated. This is shown in equation (1),

$$\left(\frac{\partial}{\partial t}+\mathbf{u}\cdot\nabla\right)\mathbf{u}+2\boldsymbol{\Omega}\times\mathbf{u}+\boldsymbol{\Omega}\times(\boldsymbol{\Omega}\times\mathbf{r}) = \nabla\cdot\left(\frac{\mu}{\rho}\nabla\mathbf{u}\right)-\frac{\nabla P}{\rho}-\mathbf{g}+\frac{\mathbf{F}}{\rho}, \quad (1)$$

where $\mathbf{u}$, $\boldsymbol{\Omega}$, $\mathbf{F}$, P, ρ, t, μ, and $\mathbf{g}$ are the velocity vector, rotational vector, body force, pressure, density, time, viscosity and gravitational acceleration, respectively.

In equation (1), the third term on the left hand side is the centrifugal force and acts as an artificial gravity. High gravity condition can be achieved by increasing the rotational velocity. Additionally, the effect of the Coriolis force (the second term on the left hand side) becomes large as the rotation rate increases. This effect becomes especially dominant for fluid flow for molten metals and semiconductors which have a low Prandtl number and large flow velocity.

Growth of a semiconductor crystal on a centrifuge has been attempted in order to improve crystal quality. Müller *et al.* reported that impurity striation in grown semiconductor crystals disappeared in the vertical Bridgman system [1] and in horizontal zone melting [2] on a centrifuge. Rodot *et al.* grew $Pb_{0.83}Sn_{0.17}Te$ crystals by using the vertical Bridgman method on a centrifuge [3]. They reported that the effects of convection on segregation disappeared at a special rotation rate (N_s). Except for this rotation rate, at higher or lower rotation rate than N_s, crystal quality was deteriorated by convective flow. Numerical and experimental studies have been performed to explain this stabilization effect. The stabilization effect in centrifuge is attributed to various reasons; i.e. (i) coincidence of isothermal plane and isocentrifugal plane [4], (ii) existence of centrifugal force gradient [5], and (iii) stabilization effect of the Coriolis force [6,7].

The above mentioned crystal growth experiments have mainly utilized a temperature gradient parallel to the direction of the effective gravitational force. This means that it is difficult to separate the effect of the Coriolis force from the other effects on flow stabilization in experimental and numerical studies. Therefore, employment of a line heat source set parallel to the effective gravitational acceleration in a centrifuge is one of the simplest way to see the effect of the Coriolis force on heat transfer. Through the transient hot-wire heating experiment, it was found that temperature increase is dependent on the configuration of the measurement cell [8].

The purpose of the present study is to clarify the effects of Coriolis forces on fluid flow in the transient hot-wire cell in a centrifuge by changing the spatial configurations of the fluids.

2. EXPERIMENT

In this section, the results of transient wire-heating experiment in the centrifuge are briefly reviewed as a motivation of the present numerical study. As we have reported elsewhere, the transient hot wire technique was applied on the centrifuge of the Tsukuba Space center of NASDA (National Space Development Agency of Japan) [8]. The thermal conductivity measurement facility, TCMF [9], was put on the cen-

NOMENCLATURE

a	centrifugal force	t	time
C_p	heat capacity	**u**	velocity.
F	body force		
$\mathbf{F}_c$	Coriolis force		
g	gravitational acceleration	Greek symbols	
$\mathbf{g}_{eff}$	effective gravitational acceleration	θ	angle
L	arm length of centrifuge	λ	thermal conductivity
N_s	critical rotation rate	μ	viscosity
P	pressure	ρ	density
r	position vector	$\boldsymbol{\Omega}$	rotational vector.

trifuge. The set angle of the fluid container was adjusted using a wedge, so that the direction of the effective force, which is the sum of normal gravity and centrifugal force, was parallel to the hot wire as shown in Fig. 1. Figure 2 shows the arrangement of the equipment used in the hot wire experiment. A carbon crucible was filled with mercury and the alumina substrate on which the wire was fabricated by printing. Constant heat flux was supplied to the specimen by the electric current passing through the wire. Consequently, the temperature of the wire increased. The average temperature of the wire was measured by detecting the change in electrical resistivity as reported in previous work [9]. Figure 3 shows the three configurations, A, B, and C, used in the experiment. During the experiment the temperature of the center region near the hot wire was always higher than other regions. Because of this, the fluid was moved up along the hot wire by the resulting force of the gravitational and centrifugal forces. Therefore, the direction of the Coriolis force near this region was constant in reference to rotation direction, as shown by $\mathbf{F}_c$ in Fig. 3. However, the relative direction of the force is different depending on configuration of the specimen. In configuration A, this force pushes the melt to the substrate, which is opposite to the direction of the force in configuration C. In configuration B the force is parallel to the surface of the substrate.

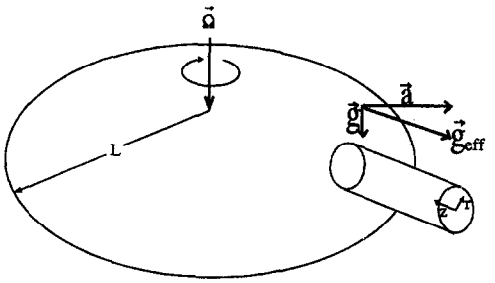

FIG. 1. Schematic diagram of the centrifuge and the hot wire equipment. (**g**: gravitational force; **a**: centrifugal force; $\mathbf{g}_{eff}$ effective force.)

Figure 4 shows the experimentally obtained temperature increases for configurations A, B, and C, which have the same centrifugal acceleration ($5g$) and the same heat flux (3.15 W cm^{-1}). Line X shows the temperature increase obtained from the experiment in which the equipment was put horizontal to the ground and the hot wire was on top of the mercury. The convection was suppressed in this case. The tendencies

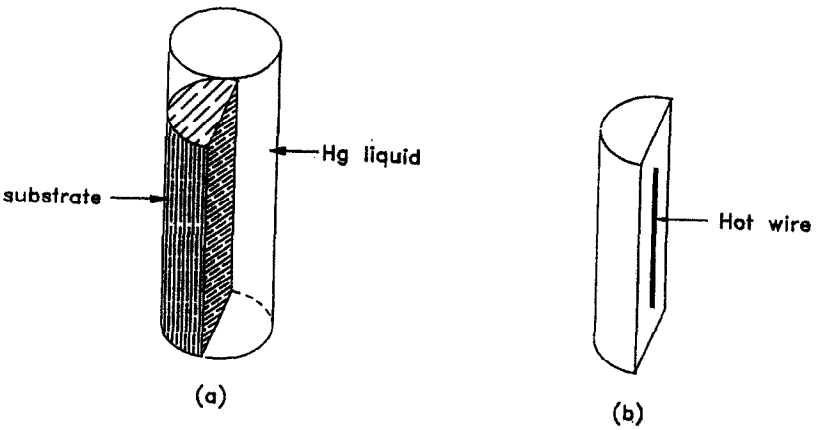

FIG. 2. Sketches of the hot wire experimental specimen (a) and the position of the hot wire on the substrate (b).

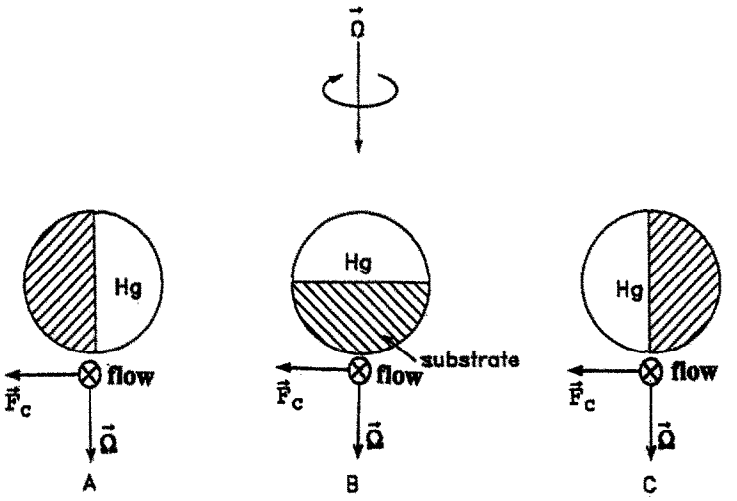

FIG. 3. Configurations of the substrate and the fluid regions of the equipment shown from the edge of the centrifuge. The direction of the Coriolis force near the hot wire is also shown by F_c. (⊗: Flow direction.) A: Substrate is in front of the melt. B: Substrate and melt are parallel. C: Melt is in front of the substrate.

of the temperature increase change as the configuration changes. The deviation from line X represents enhancement of the convective heat transfer. It is shown from the experiment that in the first stage the order of the deviation is A < B < C. Figure 5 shows the change of the apparent thermal conductivities calculated from the experimental results for configurations A, B, and C using the equation derived by Takegoshi *et al.* [10]. The effect of convective contribution to heat transfer is included in this apparent thermal conductivity. Actually, because the values of the thermal conductivity of the mercury and the alumina substrate are nearly constant during the experiment, the excess value directly represents the contribution of convective heat transfer.

The values of the apparent thermal conductivities were also different from one another. This suggests that the velocity fields for configurations A, B, and C were not the same. The order of the convection effect is proportional to the magnitude of the effective conductivity. In the first stage, the order becomes A < B < C. Because the other conditions were the same, these differences should be due to the different effects of the Coriolis force. The other experimental results for different effective gravity or different input power showed the same trends as the above result. A more detailed description of the experimental results is presented in another paper [11].

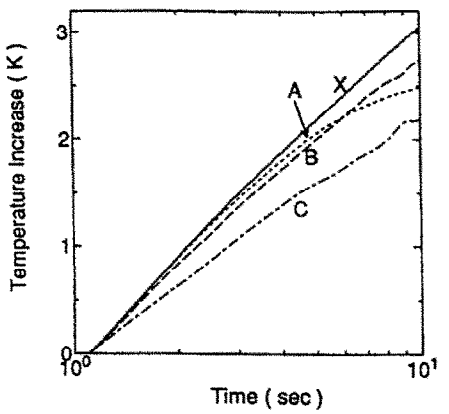

FIG. 4. Temperature increase curve obtained from experiment: the rotational acceleration is $5g$ and heat input is 3.15 W cm^{-1}.

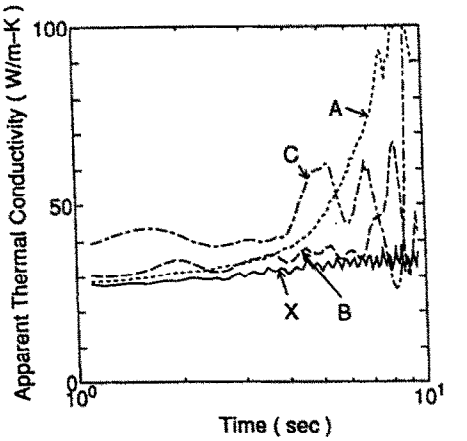

FIG. 5. Apparent thermal conductivity obtained from the results of Fig. 4.

3. NUMERICAL SIMULATION

3.1 *Governing equations and numerical schemes*

In order to explain the above mentioned experimental results, a numerical study was carried out. It was assumed that the viscosity and conductivity of the fluid was constant and the density varied linearly with temperature. The five variables (three components of the velocity, temperature and pressure) were calculated by simultaneously solving the equations shown below,

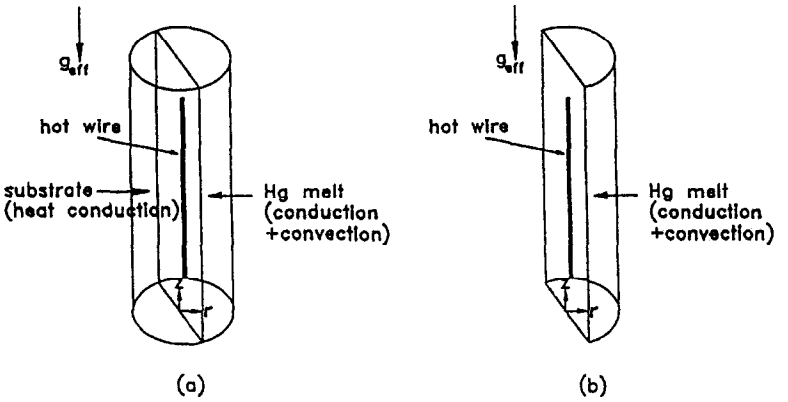

FIG. 6. (a) Domain for the calculation of type I. (b) Domain for the calculation of type II.

$$\rho\frac{\partial \mathbf{u}}{\partial t}+\rho\mathbf{u}\cdot\nabla\mathbf{u}=-\nabla P+\mu\nabla^2\mathbf{u}+\rho\mathbf{g}_{\text{eff}}-2\rho\boldsymbol{\Omega}\times\mathbf{u}, \quad (2)$$

$$\nabla\mathbf{u}=0, \quad (3)$$

$$\rho C_p\left(\frac{\partial T}{\partial t}+\mathbf{u}\cdot\nabla T\right)=\lambda\nabla^2 T, \quad (4)$$

where T, C_p, μ, and λ are temperature, heat capacity, viscosity and thermal conductivity, respectively. Pressure is calculated from the continuity equation (equation (3)) by using the SIMPLER algorithm [12].

A control volume method was used to discretize the equations. The grids for the velocities and for the other scalar variables such as temperature and pressure were staggered to prevent a checkerboard pressure field [12]. Calculation was carried out on the super computer SX-3 of NEC Corporation.

3.2. *Calculation domain and boundary conditions*

The direction of the measurement cell axis in the present calculation was assumed to be parallel to the rotational plane. Based on this assumption, the direction of the rotational vector ($\boldsymbol{\Omega}$) and the hot wire in the cell were orthogonal. The calculated domain was simplified, as shown in Fig. 6. Half of the cylinder was assumed to be filled with alumina substrate and the other half with mercury, although an entire cylinder was filled with mercury in the upper region of the experimental equipment as shown in Fig. 2(a).

Momentum equations were solved in the half cylinder (only in the melt): however, an energy equation was calculated for the full cylinder including the alumina substrate (type I calculation) or for the melt region only (type II calculation). All of the boundaries were treated as non-slip walls for the momentum equations and assumed to have a constant temperature for the energy equation of the type I calculation. The substrate wall was assumed to be adiabatic and the other boundaries were assumed to have a constant temperature for the energy equation of the type II calculation. Constant heat input was supplied along the center line, i.e. hot wire. The initial temperature was set to be the same as the boundary temperature and the initial velocities were set at 0. The thermophysical properties are listed in Table 1.

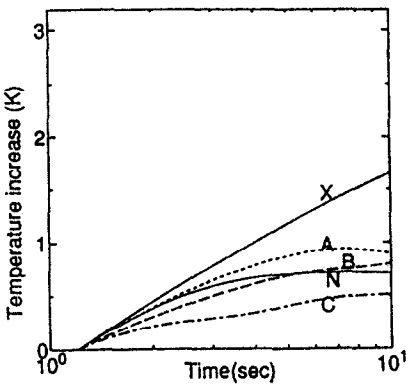

FIG. 7. Temperature increase curve obtained from calculation of type I of the same effective gravity ($5g$).

Table 1. The thermophysical properties of mercury and alumina used in this calculation

Property	Hg	Al_2O_3
Density (kg m^{-3})	13534	397
Thermal conductivity (J m^{-1} $s^{-1}\cdot K^{-1}$)	8.34	24
Heat capacity (J $kg^{-1}\cdot K^{-1}$)	138.8	800
Viscosity (kg $m^{-1}\cdot s^{-1}$)	0.00156	
Volumetric expansion coefficient (K^{-1})	1.82×10^{-4}	

THE RESULTS OF THE CALCULATION

4.1. *Type* I *calculation*

Figure 7 shows the calculated tendency of temperature increase along the hot wire. These values were the average value of the control volumes in which heat was supplied. The effective gravity was set at $5g$ and the heat input was 3.15 W cm^{-1}, which are the same as the experimental conditions in Fig. 4. Configurations A, B, and C are the same as the experimental ones. When convection in the melt is ignored, i.e. only the heat conduction problem is solved, the temperature increase shows a straight line like line X. It is certain that the deviation from this line is due to the enhancement of heat transfer by the convection. When the effect of the Coriolis force is ignored, and only centrifugal force is taken into account, the temperature increase is presented as curve N. This curve also differs from the results of A, B, and C, in which the Coriolis force is considered. The order of magnitude of the deviation from line X is A < B < C, which is the same as the experimental one.

Figure 8(a) shows velocity profiles on three planes for configuration A, 10 s after heating was started. The

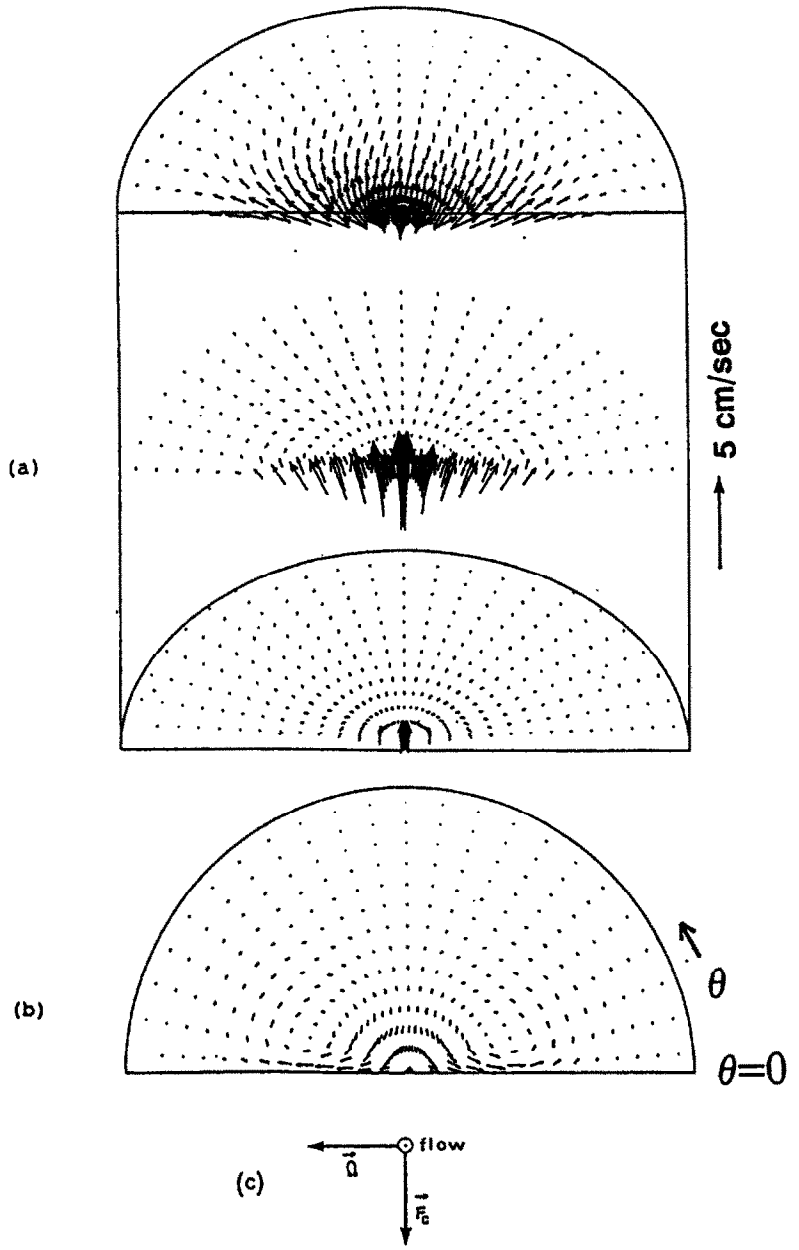

FIG. 8. Velocity profiles of selected planes and the direction of the Coriolis force of configuration A. (a) Bird's eye view; (b) top view of the middle plane of (a); (c) the directions of the velocity, rotational vector, and the Coriolis force just near the hot wire.

velocities near the center are large and the velocities of other regions are very small. Figure 8(b) shows the top view of the velocity field on the middle plane of Fig. 8(a). The fluid moves to the hot wire in the region of $\theta = 90°$ on the r–θ plane and goes out to the outer wall near the substrate surface. Figure 9 shows the velocity profiles of the same planes in the case of configuration C. The radial and azimuthal velocities are larger than those of A. The directions of the radial velocities near the hot wire are the opposite of configuration A. In each configuration, the flow is moving upward near the center, i.e. hot wire, and moving downward near the outer wall. However, the profiles of the radial or azimuthal velocities are quite different. These differences are caused by the Coriolis force. Figures 8(c) and 9(c) show the direction of the Coriolis force for configurations A and C. In configuration A, force acts toward the substrate wall near the hot wire and pushes the melt to the substrate wall. The flow driven by this force is not well developed because of the substrate wall. On the other hand, in configuration C the direction of the Coriolis force is the opposite and pulls the melt inward near the hot wire. The velocity component of this direction becomes

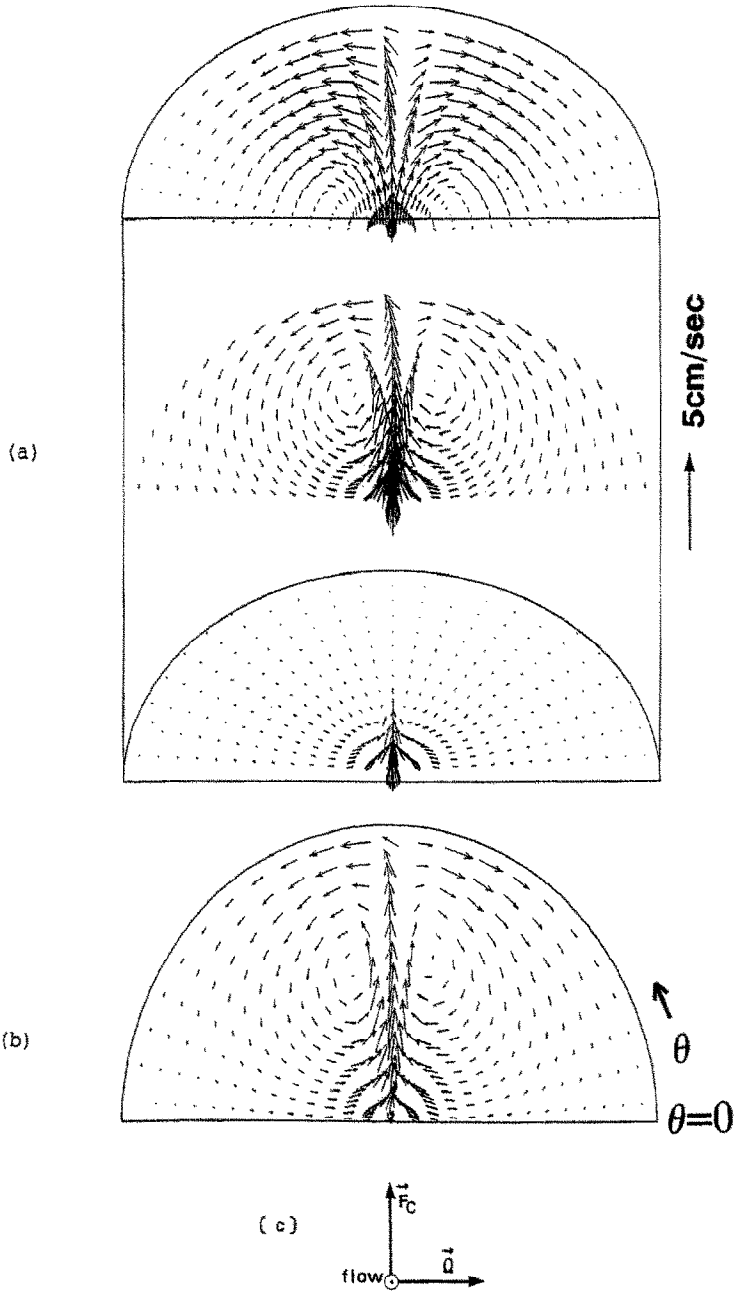

FIG. 9. Velocity profiles of selected planes and the direction of the Coriolis force of configuration C. (a) Bird's eye view; (b) top view of the middle plane of (a); (c) the directions of the velocity, rotational vector, and the Coriolis force just near the hot wire.

large because there is no obstacle in front of the force. However, the velocity component of the axial direction is decreased.

Figures 10(a) and (b) show the velocity field for configuration B. The direction of the Coriolis force is parallel to the substrate plane as shown in Fig. 10(c). The velocity field for configuration B is quite different from that for A and C. The fluid flows out near the region of $\theta = 0°$ and the velocities in this direction are larger than those for configuration A.

Figures 8–10 show that the effect of the Coriolis force depends on the configuration. The difference of the flow field caused by the force may be the main reason for the difference in temperature increase as shown in Fig. 4 (experimental results) and Fig. 7 (calculation results). Because heat transfer from the hot wire depends directly on the velocities near it, it is necessary to analyze the velocities of the grids located just near the centerline.

Figure 11 shows the change of the average value of the axial velocity along the hot wire. The heat input and effective gravity are the same as the values in Fig. 7. The Coriolis force decreases the axial velocities and the values for configurations B and C are smaller than

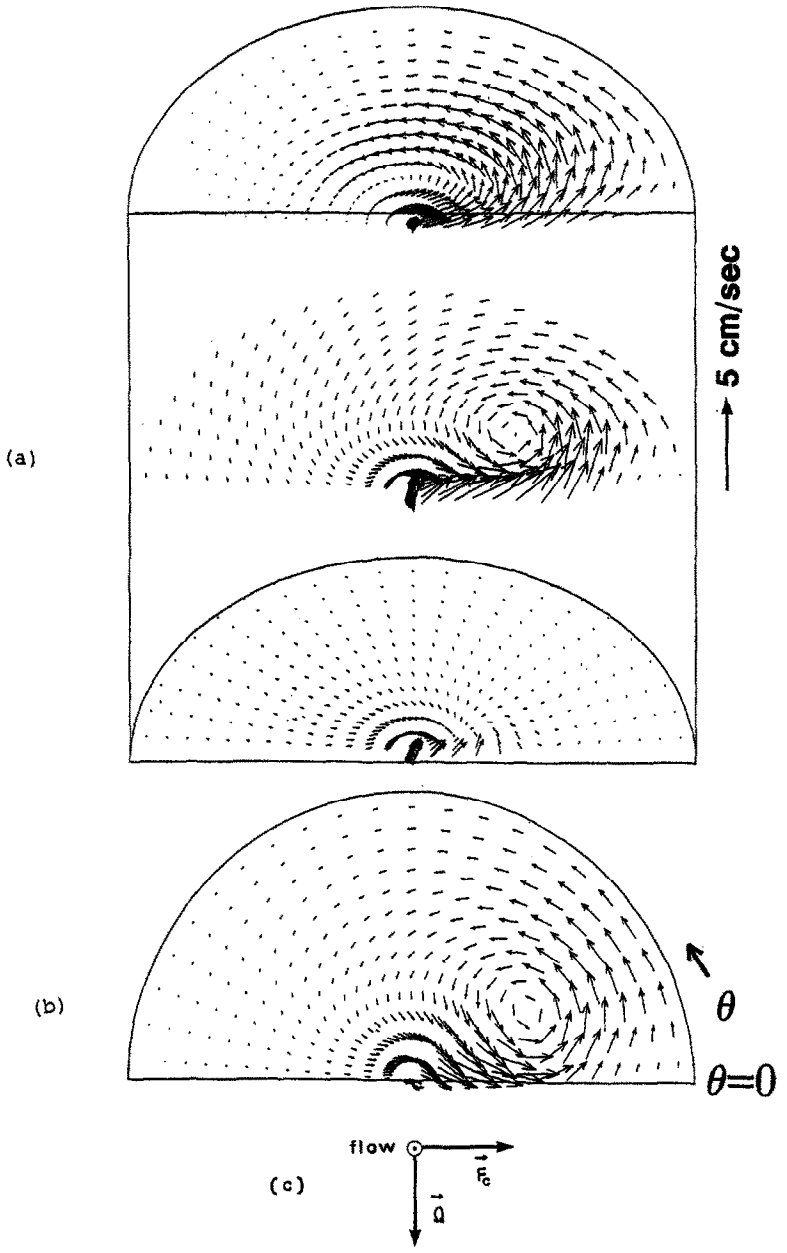

FIG. 10. Velocity profiles of selected planes and the direction of the Coriolis force of configuration B. (a) Bird's eye view; (b) top view of the middle plane of (a); (c) the directions of the velocity, rotational vector, and the Coriolis force just near the hot wire.

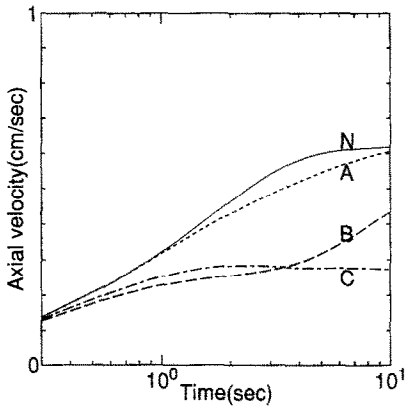

FIG. 11. Change of the average value of the axial velocities along the hot wire of type I.

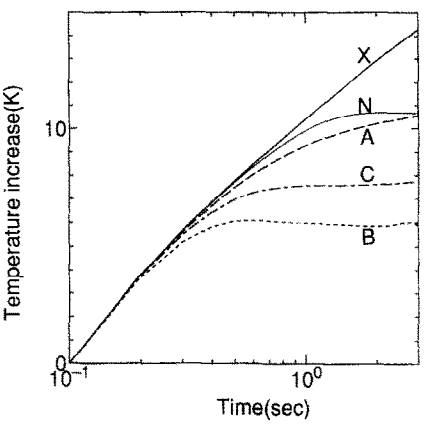

FIG. 13. Temperature increase curve obtained from calculation of type II of the same effective gravity ($5g$).

those for A. Figure 12 shows the change of the average value of the radial velocity along the hot wire. If the Coriolis force is ignored (case N), the value of this velocity component is very small. This component is produced by the Coriolis force and the order of the value of the component becomes A < C < B. Because the hot wire was very thin and long (width = 0.1 mm, length = 7 cm), most of its heat transfer to the melt occurred in the radial directions. Therefore, the amount of heat transfer by convection also depends on the radial component of the velocity. However, the order of the value of radial velocity is different from the order of the value of the effective conductivity of the experiment for configurations B and C.

4.2. *Type* II calculation

The effective gravity and the boundary conditions, except at the substrate surface, are the same as in the type I calculation. The substrate surface was treated as an adiabatic wall during this calculation. Figures 13–15 show the change of the average values of temperature, axial velocity, and radial velocity along the hot wire, respectively. The temperature increase of the results from the type II calculation differ in three ways from those for the type I calculation. Additionally,

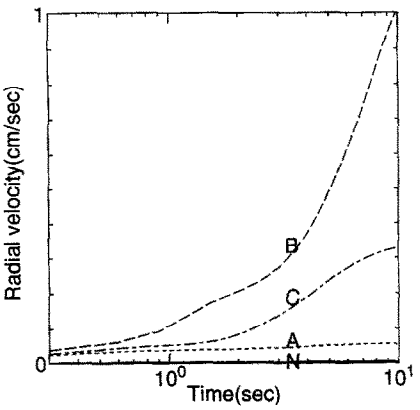

FIG. 12. Change of the average value of the radial velocities along the hot wire of type I.

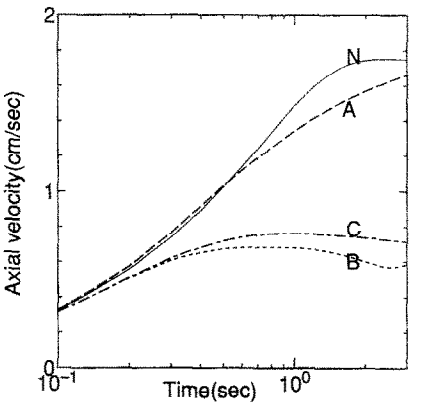

FIG. 14. Change of the average value of the axial velocities along the hot wire of type II.

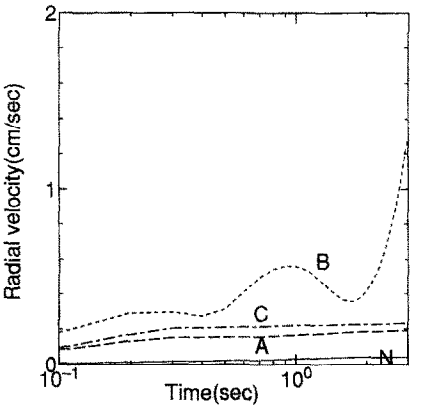

FIG. 15. Change of the average value of the radial velocities along the hot wire of type II.

the order of the amount of the deviation changes to A < C < B. On the other hand, the order of the average velocities for the type I and type II calculations are nearly the same. The profiles of the velocities were similar to those for the same configurations in the type I calculation. The order of the temperature deviation and the magnitude of the radial velocity were the same values for type II calculation. The heat transfer near

the hot wire was determined by the convection and conduction of the melt because the substrate surface was assumed to be an adiabatic wall in the type II calculation. Therefore, it is possible to say regardless of boundary conditions that the order of the effect of the Coriolis force on the radial heat transfer is $A < C < B$.

4.3. *Effects of Coriolis force on heat transfer*

The experiment and the calculation showed that the effect of the Coriolis force is large. The Coriolis force promotes heat transfer by increasing the velocities of the normal directions of the effective gravity in the hot wire experimental system, and decreases the velocity component of the direction of the effective gravity. These effects also depend on the configuration. The value of the radial velocity was largest for configuration B and the axial velocity for configurations A, respectively. This means that, with regard to axial directions, the heat transfer is largest for configuration A.

The order of the temperature deviation of type II calculation, i.e. the value of the apparent thermal conductivity, is different from those of the experiment and the type I calculation. This is caused by the heat transfer between the substrate and the melt. Because the conductivity of the substrate (alumina) is nearly three times larger than the melt (see Table 1), the temperature of the substrate is higher than the melt near the interface and heat flows from the former to the latter. This heat transfer is produced by the convective heat transfer and the strong convection of the radial directions of configuration B moves heat to the hot wire region. Because of this, the temperature checked by the hot wire for configuration B is higher than that for configuration C.

There are two factors which possibly determine the effect of the Coriolis force. The first is the direction of the specimen. The difference in configurations A and C is that the relative direction of the Coriolis force is opposite. The effect of the Coriolis force is larger in configuration C than in configuration A. The second is the characteristic length along the direction of the Coriolis force. The sizes of the specimen are same. However, the characteristic length along the direction of the Coriolis force for B is longer than for A and C. Because of this, the effect of the Coriolis force for configuration B is larger than the others.

5. CONCLUSION

The effect of the Coriolis force in the centrifuge is large and depends on the configurations. This force increases the velocity components normal to the effective gravity direction and reduces the velocity component parallel to this direction. The amount of the heat transfer is also changed by this change of convection. The magnitude of the effect of the Coriolis force depends on the configuration of the specimen and the characteristic length of the specimen. The contribution of the substrate to the heat transfer in the hot wire system is also so large that the order of the radial heat transfer of each configurations is able to be changed depending on the conductivities of the substrates.

REFERENCES

1. G. Müller, E. Schmidt and P. Kyr, Investigation of convection in melts and crystal growth under large internal accelerations, *J. Crystal Growth* **49**, 387–395 (1980).
2. G. Müller and G. Neumann, Suppression of doping striations in zone melting of InSb by enhanced convection on a centrifuge, *J. Crystal Growth* **59**, 548–556 (1982).
3. H. Rodot, L. L. Regel and A. M. Turtchaninov, Crystal growth of IV–VI semiconductors in a centrifuge, *J. Crystal Growth* **104**, 280–284 (1990).
4. W. A. Arnold, L. L. Regel and W. R. Wilcox, *Proc. The Second International Workshop on Materials Processing in High Gravity*, Potsdam NY, June 1993 (to be published).
5. A. Chevy and P. William, *Proc. The Second International Workshop on Materials Processing in High Gravity*, Potsdam NY, June 1993 (to be published).
6. W. Weber, G. Neumann and G. Müller, Stabilizing influence of the Coriolis force during melt growth on a centrifuge, *J. Crystal Growth* **100**, 145–158 (1990).
7. N. Ramachandran, J. P. Downey, P. A. Curreri and J. C. Jones, Numerical modeling of crystal growth on a centrifuge for unstable natural convection configurations, *J. Crystal Growth* **126**, 655–674 (1993).
8. S. Nakamura, T. Hibiya and K. Kakimoto, Thermal conductivity measurement of mercury on a centrifuge, *J. Japan Soc. Microgravity Appl.* **8**, 204 (1991).
9. F. Yamamoto, S. Nakamura, T. Hibiya, T. Yokota, D. Grobe, H. Harms and P. Kyr, Developing a measuring system for thermal conductivity in molten semiconductors on board the TEXUS rocket, *Proc. CSME Mechanical Engineering Forum*, Toronto, pp. 1–6, June (1990).
10. E. Takegoshi, S. Imura, Y. Hirasawa and T. Takenaka, A method of measuring the thermal conductivity of solid materials by transient hot wire method of comparison, *Bull. JSME* **25**, 395–402 (1982).
11. T. Hibiya, S. Nakamura, K.-W. Yi and K. Kakimoto, Application of transient hot-wire technique on centrifuge, *Proc. The Second International Workshop on Materials Processing in High Gravity*, Potsdam NY, June 1993 (to be published).
12. S. V. Patankar, *Numerical Heat Transfer and Fluid Flow*. McGraw-Hill, New York, 1980.